Structural Engineering and Mechanics, Vol. 39, No. 6 (2011) 795-812
DOI: http://dx.doi.org/10.12989/sem.2011.39.6.795

Fragility analysis of R/C frame buildings based on different types of hysteretic model

Muzaffer Borekci* and Murat S. Kirçil[a]

Department of Civil Engineering, Yildiz Technical University, Istanbul, Turkey

(Received May 31, 2010, Accepted June 22, 2011)

Abstract. Estimation of damage probability of buildings under a future earthquake is an essential issue to ensure the seismic reliability. Fragility curves are useful tools for showing the probability of structural damage due to earthquakes as a function of ground motion indices. The purpose of this study is to compare the damage probability of R/C buildings with low and high level of strength and ductility through fragility analysis. Two different types of sample buildings have been considered which represent the building types mentioned above. The first one was designed according to TEC-2007 and the latter was designed according to TEC-1975. The pushover curves of sample buildings were obtained via pushover analyses. Using 60 ground motion records, nonlinear time-history analyses of equivalent single degree of freedom systems were performed using bilinear hysteretic model and peak-oriented hysteretic model with stiffness – strength deterioration for each scaled elastic spectral displacement. The damage measure is maximum inter-story drift ratio and each performance level considered in this study has an assumed limit value of damage measure. Discrete damage probabilities were calculated using statistical methods for each considered performance level and elastic spectral displacement. Consequently, continuous fragility curves have been constructed based on the lognormal distribution assumption. Furthermore, the effect of hysteresis model parameters on the damage probability is investigated.

Keywords: earthquake damage; fragility curves; hysteretic models; degradation

1. Introduction

Estimation of the potential damage of a building under the effect of future earthquakes is an essential issue. However the building stock has many buildings and estimating the potential damage of every building takes long time and gets expensive. Fragility curves can be used to overcome those difficulties. Using probabilistic methods to estimate the potential damage of a building is reasonable since earthquakes which will be occurred in the future cannot be defined with all their characteristics. Fragility curves are useful tools for showing the probability of structural damage due to earthquakes as a function of ground motion indices, e.g., peak ground acceleration (PGA), peak ground velocity (PGV), elastic pseudo spectral acceleration (S_a), elastic spectral displacement (S_{de}). The purpose of this study is to compare the damage probability of R/C buildings with low and high level of strength and ductility through fragility analysis. Two different types of sample R/C

*Corresponding author, Ph.D. Student, E-mail: mborekci@yildiz.edu.tr
[a]Assistant Professor, E-mail: kircil@yildiz.edu.tr

buildings have been considered within the scope of this study. The first one (Building A) was designed according to 2007 version of Turkish Earthquake Code (TEC) which represents a building with high ductility and strength and the latter (Building B) was designed according to 1975 version of TEC which represents a building with low ductility and strength. 2007 version of TEC enforces engineers to design structures with high ductility relative to 1975 version of it. Inelastic displacement demand (S_{di}) of an earthquake from a building is an important and basic data especially for the evaluation of seismic safety of the existing buildings. Most of codes and guides consider the inelastic displacement of an equivalent single degree of freedom system as an indicator of the seismic demand of an existing building. Thus, spectral displacement of equivalent single degree of freedom system (SDOF) is selected as the parameter that represents the seismic demand of a structure for developing the fragility curves. Furthermore, using equivalent SDOF system instead of multi degree of freedom system allows clearer observations for the effect of hysteretic parameters on damage probability. In this study, inelastic displacement demand (S_{di}) was determined by nonlinear dynamic analysis of equivalent SDOF system. Bilinear hysteretic model and strength – stiffness deteriorated model were used for nonlinear dynamic analysis so that the effect of hysteretic model on damage probability can be investigated. 60 ground motion records were considered for nonlinear time history analysis to determine inelastic displacement demand and maximum inter-story drift ratio was used as the damage indicator with respect to inelastic displacement demand. Each performance level, considered in this study, has an assumed limit value of inter-story drift ratio. Fragility curves were developed based on these assumed limits of inter-story drift ratio.

2. Fragility curves

Fragility curves show the probability of reaching or exceeding a specific limit state at a given level of ground shaking intensity. A limit state usually represents a damage condition, or a limitation of usage. Limit states can be defined in terms of inter-story drift ratio, strain or plastic rotation (Maniyar *et al.* 2009).

Erberik and Elnashai (2003) explained different methodologies which may be utilized for derivation of fragility curves in their study. The first one is *empirical fragility curves* which are based on available damage data from previous earthquakes. The second one is *judgmental fragility curves*. This approach is based on expert opinions when there is not enough data to develop fragility curves. The third one is *analytical fragility curves.* The fragility curves which are constructed using this approach are based on engineering analysis. Probability is obtained using damage distributions simulated from analyses of structural models under increasing earthquake intensity. The last method is *hybrid fragility curves* (Jeong and Elnashai 2007b). Hybrid methods attempt to compensate for the scarcity of observational data, subjectivity of judgmental data and modeling deficiencies of analytical procedures by combining data from different sources. In this study, analytical method is used to construct the fragility curves.

3. Hysteretic models

In this study fragility curves were constructed based on both bilinear and stiffness-strength deteriorated Peak-Oriented hysteretic models and the effects of the cyclic deterioration on the

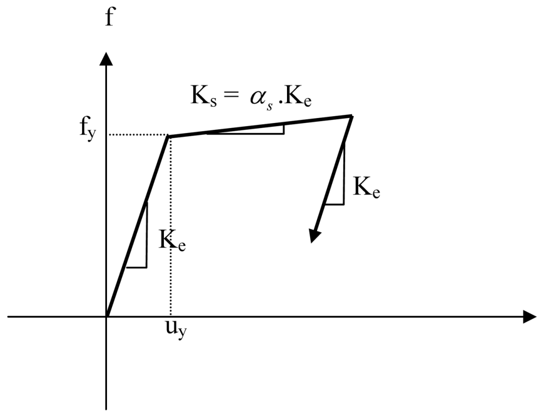

Fig. 1 Backbone curve of the bilinear hysteretic model

damage probability were investigated through fragility curves.

3.1 Bilinear model

A finite slope is assigned to the stiffness after yielding to simulate the strain hardening characteristics of the steel and the reinforced concrete (Otani 1981). The backbone curve of the bilinear model was shown in Fig. 1.

The parameters in the backbone curve are elastic (initial) stiffness K_e, post-yield stiffness $K_s = \alpha_s \cdot K_e$, yield strength f_y and yield displacement u_y, respectively. Backbone curve can be defined by using three parameters K_e, K_s and f_y.

3.2 Peak-oriented model

This model keeps basic hysteretic rules proposed by Clough and Johnston (1966) and later modified by Mahin and Bertero (1975), but the backbone curve is modified by Ibarra *et al.* (2005) to include strength capping and residual strength as shown in the Fig. 2 (Ibarra *et al.* 2005). In

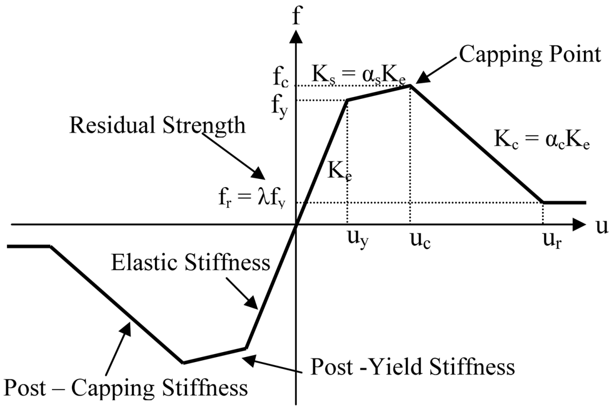

Fig. 2 Backbone curve for deteriorated model (Ibarra *et al.* 2005)

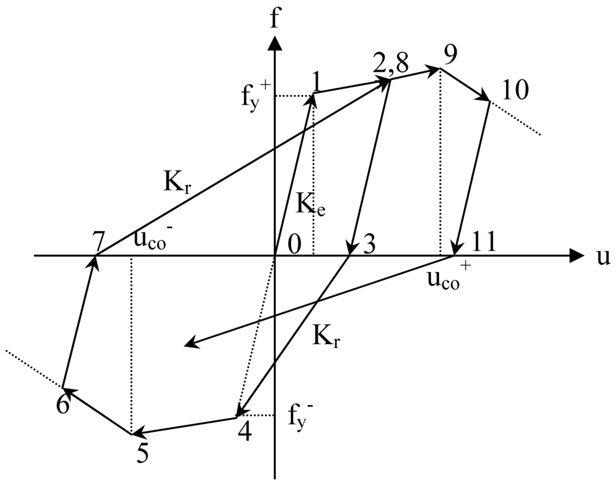

Fig. 3 Basic rules for peak-oriented hysteretic model (Ibarra *et al.* 2005)

Fig. 2, K_e is the elastic (initial) stiffness, f_y is the yield strength, f_r is the residual strength, f_c is the maximum strength, K_s is the post – yield stiffness, u_y is the yield displacement, u_c is the beginning of a softening branch which is called cap displacement, K_c is the post – capping stiffness which usually has a negative value.

When the loading path reaches the horizontal axis, the loading goes through reloading path. The basic idea of the peak-oriented model is that the reloading path always targets the previous maximum displacement. The basic rules of Peak-Oriented Model can be seen in Fig. 3.

3.3 Energy based cyclic deterioration

Four different deterioration modes can be occurred after the loading path reaches the yielding point at least one direction. These deterioration modes are *basic strength deterioration, post – capping strength deterioration, unloading stiffness deterioration* and *reloading stiffness deterioration.* Detailed information can be seen in the study of Ibarra *et al.* (2005). An example of considered hysteresis loop is given in Fig. 4 which shows the combination of all deterioration modes.

It is assumed that the deterioration in excursion i is defined by a deterioration parameter β_i.

$$\beta_i = \left(\frac{E_i}{E_t - \sum_{j=1}^{i} E_j} \right)^c \tag{1}$$

E_i is the hysteretic energy dissipated in excursion i, E_t is the hysteretic energy dissipation capacity, ΣE_j is the hysteretic energy dissipated in all previous excursions, c is the component which defines the rate of deterioration.

The hysteretic energy dissipation capacity is determined by following equation

$$E_t = \gamma f_y u_y \tag{2}$$

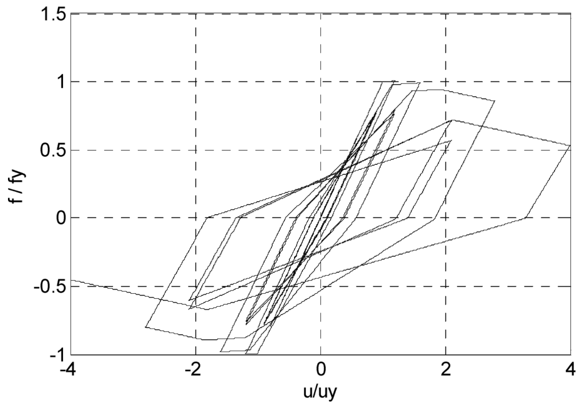

Fig. 4 An example of Peak-Oriented hysteretic model which shows the combination of all deterioration modes

γ expresses the hysteretic energy dissipation capacity as a function of twice the elastic strain energy at yielding ($f_y u_y$). For c which is the rate of the deterioration, reasonable range is between 1.0 and 2.0 (Rahnama 1993). The value of 2.0 slows down the rate of deterioration in early cycles and accelerates the rate of deterioration in later cycles, whereas a value of 1.0 implies an almost constant rate of deterioration. Throughout the loading history, β_i must be within the limits $0 < \beta_i \leq 1$. If β_i is outside these limits the hysteretic energy capacity is exhausted and collapse is assumed to take place (Ibarra *et al.* 2005).

4. Sample buildings

Two different types of 5-storey sample building have been considered within the scope of this study. The buildings were named as Building A and Building B, respectively. Building A was designed according to TEC-2007 and Building B was designed according to TEC-1975. The buildings are R/C frames and both of them have same storey height, span length and beam dimensions. The dimensions of two buildings are shown in Fig. 5. Column dimensions, column and beam reinforcement ratios and materials are different for each building. For simplicity, the buildings are symmetric in plan and they have three spans in horizontal direction. This symmetric plan allows the use of two dimensional structural models. As mentioned earlier Building A represents a building with high level of strength and ductility. Thus, it complies with design rules which provide ductility to structures such as strong column-weak beam, capacity design for shear reinforcement, low spacing of shear reinforcement, compressive reinforcement for beam sections etc.

5. Material properties

Jeong and Elnashai (2007a) showed that mean of the earthquake demand of 30 sample buildings which were produced to consider the effect of material uncertainty, is close to the earthquake demand of a building which has the mean material strength of 30 sample buildings. Thus, mean material strength was considered in this study.

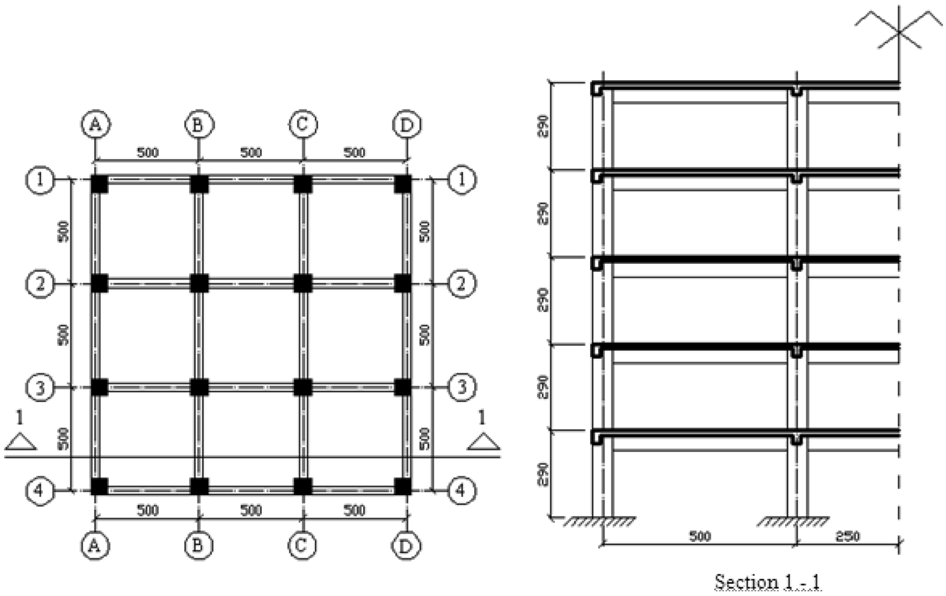

Fig. 5 Typical floor plan and elevation of A and B buildings

5.1 Material properties of building A

The concrete with characteristic compressive strength ($f_{ck,\%5}$) of 20 MPa was used for design. It is assumed that compressive strength of the concrete has a normal distribution and standard deviation of the concrete (σ) is taken to be 5 MPa (Bartlett and MacGregor 1996). Thus, mean value of compressive strength of the concrete (f_{co}) is determined with Eq. (3)

$$f_{co} = f_{ck,\%5} + z \cdot \sigma = 20 + 1.64 \cdot 5 = 28 \text{ MPa} \tag{3}$$

Grade 60 reinforcement bars were used for design and statistical distribution of the reinforcement is assumed as a lognormal distribution with mean strength of 475 MPa (Ghobarah *et al.* 1998).

5.2 Material properties of building B

The concrete with characteristic compressive strength of 14 MPa was used for design. It is assumed that compressive strength of the concrete has a normal distribution and standard deviation of the concrete (σ) is taken to be 5 MPa. Thus, mean value of compressive strength of the concrete (f_{co}) is equal to 22 MPa.

Grade 40 reinforcement bars were used for design and statistical distribution of the reinforcement is assumed as a lognormal distribution with mean strength of 337 MPa (Kwon and Elnashai 2005).

6. Selection of ground motions

A total of 60 earthquake acceleration time histories, two horizontal components at each station, with magnitudes ranging from 6 to 7.5 were used in this study. The earthquake acceleration time histories were divided into three groups according to local soil conditions at the recording station. Each group consisted of 20 ground motions. The average shear wave velocity of the first group is between 760 m/s and 1525 m/s. The second group is consisted of ground motions with average shear wave velocity between 360 m/s and 760 m/s. The last 20 ground motion records have average shear wave velocity between 180 m/s and 360 m/s. Location of the recording stations in the first group corresponds to site class A/B while the location of the recording stations in the second and third groups corresponds to site classes C and D respectively according to NEHRP classification. There are different limitations on the fault distance defined in literature to describe the near fault

Table 1 Selected ground motions (PEER Strong Motion Database)

Earthquake	Mag. (Ms)	Station Name	Station Number	Site Class	Distance (km)	PGA (g)	
						Comp1	Comp2
1971 San Fernando	6.5	Lake Hughes, Array Stat. 4	126	A/B	24	0.192	0.153
1971 San Fernando	6.5	Pasadena	266	A/B	19.1	0.089	0.202
1971 San Fernando	6.5	Lake Hughes, Array Stat. 9	127	A/B	23.5	0.157	0.134
1986 Palm Springs	6	Silent Valley, Poppet Flat	12206	A/B	25.8	0.139	0.113
1986 Palm Springs	6	Winchester, Bergman Rch.	13199	A/B	57.6	0.07	0.093
1986 N. Palm Springs	6	Murrieta Hot Springs, Colling Ranch	13198	A/B	54.8	0.053	0.049
1989 Loma Prieta	7.1	South San Francisco, Sierra Point	58539	A/B	68.2	0.056	0.105
1989 Loma Prieta	7.1	San Francisco, Telgraph Hill	58133	A/B	76.5	0.036	0.077
1994 Northridge	6.7	Lake Huges, Array Station 9	127	A/B	25.4	0.165	0.217
1994 Northridge	6.8	Antelope Buttes	24310	A/B	47.3	0.046	0.068
1971 San Fernando	6.5	Lake Hughes, Array Stat. 12	128	C	20.3	0.366	0.283
1984 Morgan Hill	6.1	Gilroy, Gavilan Coll.	47006	C	16.2	0.114	0.095
1987 Whittier	6.1	Long Beach, Recreation P.	14241	C	30.5	0.058	0.051
1987 Whittier	6.1	Sylmar, Olive View Medical Center	24514	C	47.7	0.065	0.055
1987 Whittier	5.7	Castaic Old Ridge Route	24278	C	72.2	0.071	0.056
1989 Loma Prieta	7.1	Woodside, Fire Station	58127	C	39.9	0.08	0.082
1989 Loma Prieta	7.1	Fremont - Mission San Jose	57064	C	39.5	0.124	0.106
1994 Northridge	6.8	Castaic Old Ridge Route	24278	C	22.6	0.568	0.514
1994 Northridge	6.8	San Marino,SW Academy	24401	C	35.1	0.116	0.15
1994 Northridge	6.8	Rancho Palos Verdes, Hawthorne Blvd.	14404	C	55.2	0.072	0.054
1979 Imperial Valley	6.1	Coachella, Canal#4	5066	D	49.3	0.115	0.128
1987 Whittier	6.1	Downey, County Maintenance Bldg	14395	D	16.2	0.221	0.141
1987 Whittier	6.1	Los Angeles, Hollywood Storage Bldg	24303	D	25.2	0.221	0.124
1987 Whittier	6.1	Century City, LA Country Club South	24390	D	31.3	0.051	0.063
1987 Whittier	6.1	Pomona, 4th and Locust FF	23525	D	28.8	0.067	0.056
1989 Loma Prieta	7.1	Agnews, State Hospital	57066	D	28.2	0.172	0.159
1989 Loma Prieta	7.1	Salinas	47179	D	32.6	0.091	0.112
1989 Loma Prieta	7.1	APEEL 2E Hayward Muir Sch	58393	D	52.7	0.171	0.139
1992 Landers	7.5	Hemet Fire Station	12331	D	69.5	0.081	0.097
1994 Northridge	6.8	Los Angeles, Hollywood Storage Bldg	24303	D	25.5	0.231	0.358

effect. In this study, minimum considered fault distance is 15 km so that the near fault effect can be minimized. All selected ground motions are given in Table 1.

7. Methodology

- Pushover curves and inter-story drift ratio of the sample buildings at each step of pushover analysis were determined by using IDARC 2D software package.
- Pushover curves were transformed to modal capacity diagrams by the help of modal parameters of first vibration mode of the sample buildings.
- Horizontal axis of the fragility curve is elastic spectral displacement (S_{de}). All the ground motion records were scaled to certain S_{de} and nonlinear time history analyses of equivalent single degree of freedom (SDOF) system were performed for each S_{de} to determine the inelastic spectral displacement (S_{di}). Time history analyses were performed using a MATLAB code prepared by the first author for this study.
- Time history analysis is repeated for increasing values of elastic spectral displacement using scaled ground motions.
- Inter-story drift ratios were used as damage measure.
- Inter-story drift ratio obtained from the time history analyses of SDOF systems has been increased by a factor of 1.13 (Jeong and Elnashai 2007b) to predict the inter-story drift ratio of MDOF systems. The standard deviation of this ratio is assumed 0.17 (explained in Section 11) following the results obtained by Jeong and Elnashai (2007b).
- It is assumed that inter-story drift ratios which are determined for each S_{de} have a lognormal distribution and discrete damage probabilities of exceeding the damage level were calculated.
- Consequently, continuous fragility curves were constructed from those discrete probabilities.

8. Analytical model of the sample buildings

Pushover curves and essential modal parameters were determined by analytical modeling of the buildings which were modeled by using IDARC 2D software package. Period of first vibration mode is 0.79 sec and 1.30 sec for Building A and B, respectively. Pushover curves and capacity diagrams of the sample buildings are shown in Fig. 6. In Fig. 6(a), V, W, u are base shear force, total weight and top displacement of the buildings, respectively. Fig. 6(b) and 6(c) show capacity diagrams where a and d are modal acceleration and modal displacement, respectively. a and d are determined using Eq. (4) and Eq. (5)

$$d = \frac{u}{\Phi_{N1}\Gamma_1} \tag{4}$$

$$a = \frac{V}{M_1^*} \tag{5}$$

Φ_{N1} : Top story amplitude of first vibration mode of the building
Γ_1 : Participation factor of first vibration mode
M_1^*: Effective mass of first vibration mode

Table 2 The list of the modal parameters of the first mode

Modal Parameters	T_1 (s)	Φ_{N1}	Γ_1	M_1^* (kNs^2/m)
Building A	0.79	1.477	0.878	771.1
Building B	1.3	1.751	0.788	620.65

The list of the modal parameters was given in the Table 2.

9. Parameters of bilinear hysteretic model

The parameters to identify the envelop of the hysteretic model are yielding displacement (u_y), yielding strength (f_y) and post-yield stiffness ratio (α_s) which are mentioned in Section 3.1. Those parameters were determined by capacity diagrams of sample buildings. The parameters of envelop of the bilinear hysteretic model is given in the Table 3.

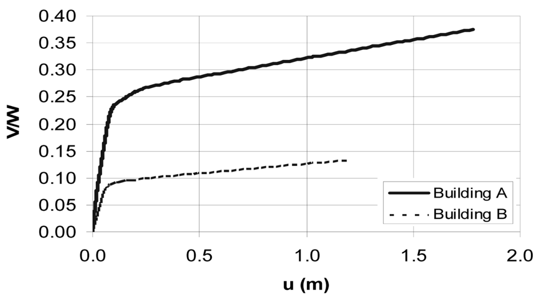

(a) Pushover curves of the buildings

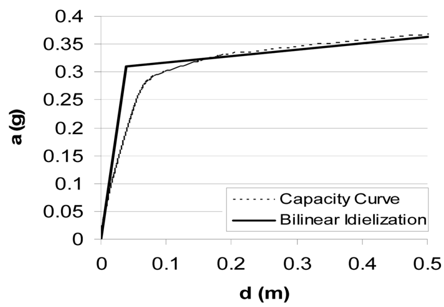

(b) Capacity diagram of Building A

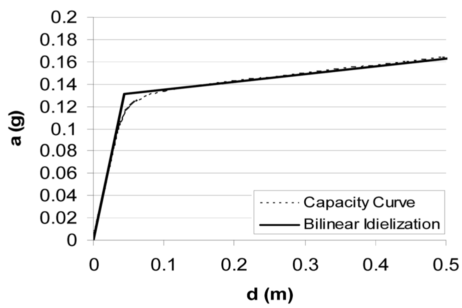

(c) Capacity diagram of Building B

Fig. 6 Pushover curves and capacity diagrams of buildings

Table 3 The parameters of envelop of the bilinear hysteretic model

	u_y (m)	f_y (kN)	α_s (%)
Building A	0.038	3.05	1.42
Building B	0.052	1.3	2.74

10. Parameters of stiffness and strength deteriorated hysteretic model

The details of this model were explained in Section 3.3. The parameters which were given in Table 3 are also used for this model.

The parameters those effect the cyclic deterioration are α_c, u_c/u_y, $\gamma_{s,c,k,a}$ (Ibarra *et al.* 2005). Although the parameter *c* effects the cyclic deterioration, Ibarra *et al.* (2005) suggested a constant value of 1 for *c* and this suggestion is followed in this study.

The coefficient of residual strength λ was assumed as 0 (λ = 0). Thus, post – capping branch can reach the horizontal axis and when the post-capping branch intersect the horizontal axis it is assumed that collapse has been occurred and the solving is ended (Ibarra 2002, Ayoub *et al.* 2009).

The parameter γ can have different values for each deterioration modes. The different indices are used for different modes. γ_s is for *basic strength deterioration*, γ_c is for *post-capping strength deterioration*, γ_u is for *unloading stiffness deterioration* and γ_a is for *accelerated reloading stiffness deterioration.* However the results which were determined by using a same value for all γ parameters is sufficient for understanding the effect of cyclic deterioration (Ibarra *et al.* 2005).

Fig. 8 shows the effect of the parameters of cyclic deteriorated model on the hysteretic response of a system subjected to the CUREE loading protocol. CUREE standard loading protocol which is shown in Fig. 7, was used as ground motion to evaluate the hysteretic behavior of deteriorated model since that loading protocol has ordinary motions. The primary objective of CUREE loading history is to evaluate capacity level seismic performance of components subjected to ordinary (not near-fault) ground motions whose probability of exceedance in 50 years is 10 percent (Krawinkler *et al.* 2000).

There are two types of strength degradation which are named as *cyclic* strength degradation and *in-cycle* strength degradation (FEMA 440 2005). The strength degradation in the negative zone is

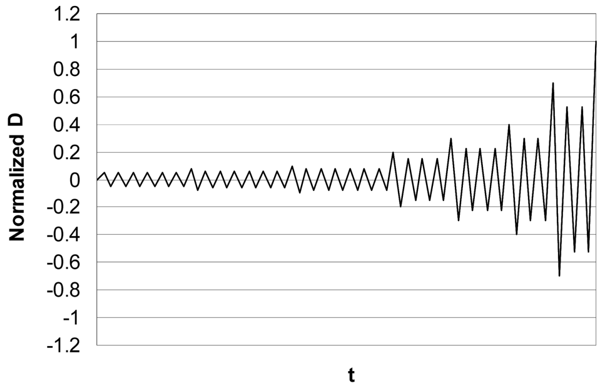

Fig. 7 CUREE standard loading protocol (Krawinkler *et al.* 2000)

Table 4 Parameters of cyclic deteriorated model and the labeling of each model

	SSD30	SSD100	SSD30M2	SSD100M2	SSD30M6	SSD100M6
γ	30	100	30	100	30	100
u_c/u_y	∞	∞	2	2	6	6
α_c	-	-	10%	10%	10%	10%

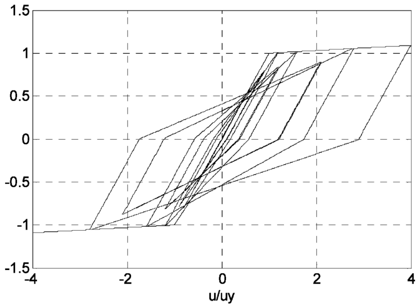

(a) $\gamma_{s,c,k,a} = \infty$, $u_c/u_y = 6$, $\alpha_c = -0.50$, $\lambda = 0$

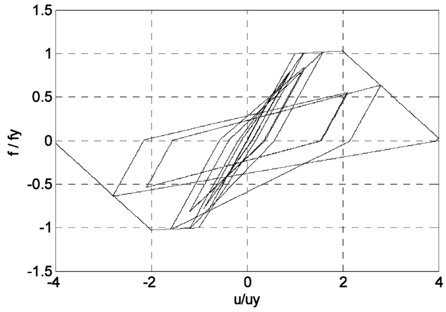

(b) $\gamma_{s,c,k,a} = \infty$, $u_c/u_y = 2$, $\alpha_c = -0.50$, $\lambda = 0$

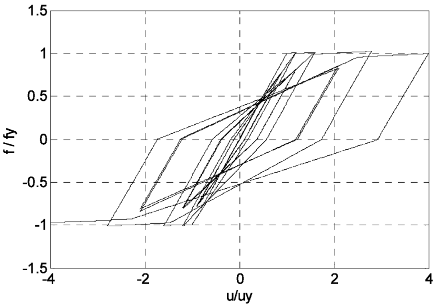

(c) $\gamma_{s,c,k,a} = 100$, $u_c/u_y = 6$, $\alpha_c = -0.50$, $\lambda = 0$

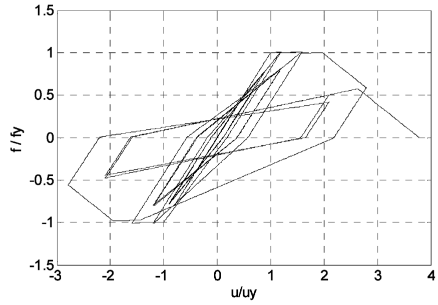

(d) $\gamma_{s,c,k,a} = 100$, $u_c/u_y = 2$, $\alpha_c = -0.50$, $\lambda = 0$

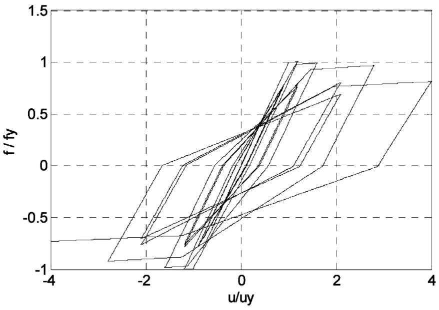

(e) $\gamma_{s,c,k,a} = 30$, $u_c/u_y = 6$, $\alpha_c = -0.50$, $\lambda = 0$

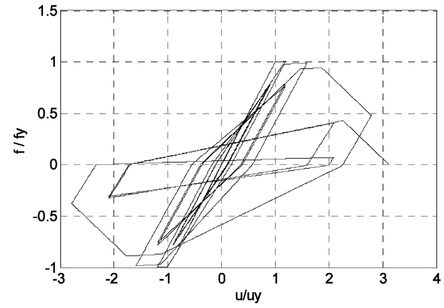

(f) $\gamma_{s,c,k,a} = 30$, $u_c/u_y = 2$, $\alpha_c = -0.50$, $\lambda = 0$

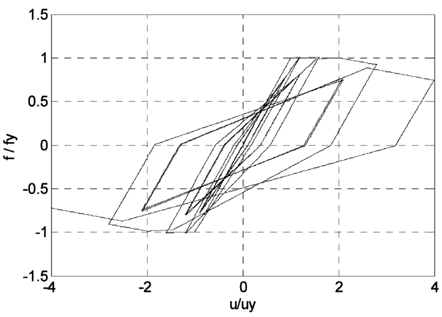

(g) $\gamma_{s,c,k,a} = 30$, $u_c/u_y = 6$, $\alpha_c = -0.10$, $\lambda = 0$

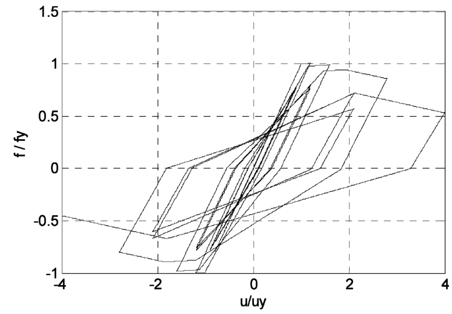

(h) $\gamma_{s,c,k,a} = 30$, $u_c/u_y = 2$, $\alpha_c = -0.10$, $\lambda = 0$

Fig. 8 Effect of the hysteretic parameters on hysteretic response of a system subjected to the CUREE loading protocol ($\alpha_s = 0.03$)

called as in-cycle strength degradation and Fig. 8(b) can be an example that type of degradation. Fig. 8(e) can be an example for the type of cyclic strength degradation. However, it is important to note that cyclic deterioration (strength and stiffness deterioration) can have both or one of those types of strength degradation.

Table 4 shows different combinations of considered parameters for deteriorated cyclic model. As an example, SSD30M2 defines the strength and stiffness degrading model with γ of 30 and ductility of 2. 7 different cyclic behaviors were considered within the scope of this study including the bilinear model (the labeling of bilinear model is **BL**).

11. Derivation of fragility curves

Fragility curves express the probability of reaching or exceeding a specific limit state at a given level of ground shaking intensity. Lognormal distribution for damage probability is a common assumption in the literature (Karim and Yamazaki 2003, Kirçil and Polat 2006, Jeong and Elnashai 2007b, Senel and Kayhan 2010). A typical fragility curve is shown in Fig. 9.

The probability of reaching or exceeding a limit state (LS) at a given earthquake intensity can be expressed as follows

$$P(\mathrm{LS}) = P[(d_{LS} \leq d_{\max})] = 1 - \Phi(r) \tag{6}$$

where d_{LS} and $d_{\max}$ are limit state capacity and maximum demand, respectively. By assuming a lognormal distribution, the standard normal variant can be expressed as follows

$$r = \frac{\ln d_{LS} - \lambda_D}{\sqrt{\zeta_{LS}^2 + \zeta_D^2}} \tag{7}$$

where λ_D is mean value with lognormal distribution and it can be expressed in terms of the mean of the maximum response ($\bar{d}_{\max}$) and its dispersion (ζ_D).

$$\lambda_D = \ln \bar{d}_{maks} - \frac{\zeta_D^2}{2} \tag{8}$$

The mean of the maximum response ($\bar{d}_{\max}$) obtained from the time history analyses of equivalent

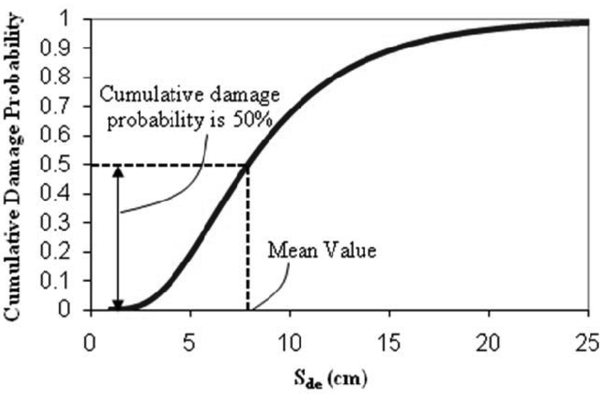

Fig. 9 A typical fragility curve

SDOF systems must be converted to the response of MDOF systems (Chenouda and Ayoub 2009, Jeong and Elnashai 2007b). Thus, inter-story drift ratios obtained from the time history analyses of SDOF systems have been increased by a factor of 1.13 (Jeong and Elnashai 2007b) to predict the inter-story drift ratio of MDOF systems.

ζ_{LS} is the lognormal standard deviation of a limit state and is assumed to be 0.3 in this study (Jeong and Elnashai 2007b).

The dispersion of maximum demand ζ_D is obtained as the combination of uncertainties associated with demand estimation

$$\zeta_D = \sqrt{\ln\left(1+\left(\frac{\sigma_r}{\bar{d}_{maks}}\right)^2\right)+\ln\left(1+\left(\frac{\sigma_c}{\bar{d}_{maks}}\right)^2\right)+\ln\left(1+\left(\frac{\sigma_m}{\bar{d}_{maks}}\right)^2\right)+\ln\left(1+\left(\frac{\sigma_D}{\bar{d}_{maks}}\right)^2\right)} \tag{9}$$

in where σ_r and σ_c are the standard deviations due to randomness in earthquake records and material properties, respectively. σ_m is the uncertainty due to the simplification of a structural model (using SDOF system instead of MDOF system) and is assumed to be 0.17 in this study (Jeong and Elnashai 2007b). σ_r is considered by using 60 earthquake records.

Jeong and Elnashai (2007a) showed that mean of the earthquake demand of 30 sample buildings which were produced to consider the effect of the material uncertainty is pretty close of the response of the building which has the mean strength value for the materials. Thus, σ_c was ignored in this study.

In this study, limit state is expressed in terms of *Immediate Occupancy, Life Safety* and *Collapse Prevention* performance levels which are defined in FEMA 356. Inter-story drift ratio is assumed as a damage indicator for the determination of the probability of exceeding those performance levels.

Limit values of inter-story drift ratio for each performance level were given in Table 5.

For each building, time history analyses were performed from 1 cm elastic spectral displacement (S_{de}) to 25 cm with the interval of 1 cm. Maximum inter-story drift ratio was determined under the effect of each ground motion which is scaled to considered elastic spectral displacement. Then, probability of exceeding of a specific performance level was determined based on inter-story drift ratios.

For one building, 1500 nonlinear time-history analyses were performed for each hysteresis type and totally 21000 nonlinear time-history analyses were performed.

The discrete probabilities were transformed to continuous form by using lognormal probability paper. A typical probability paper and transformation to continuous form of discrete probabilities are shown in Fig. 10.

Standard normal variant can be expressed generally as

$$r = \frac{\ln X - \lambda}{\zeta} \tag{10}$$

Eq. (10) is arranged as follows

$$\ln X = \zeta r + \lambda \tag{11}$$

Table 5 Limit values of inter-story drift ratio for each performance level (FEMA 356)

	Immediate Occupancy	Life Safety	Collapse Prevention
Inter-story drift ratio	1%	2%	4%

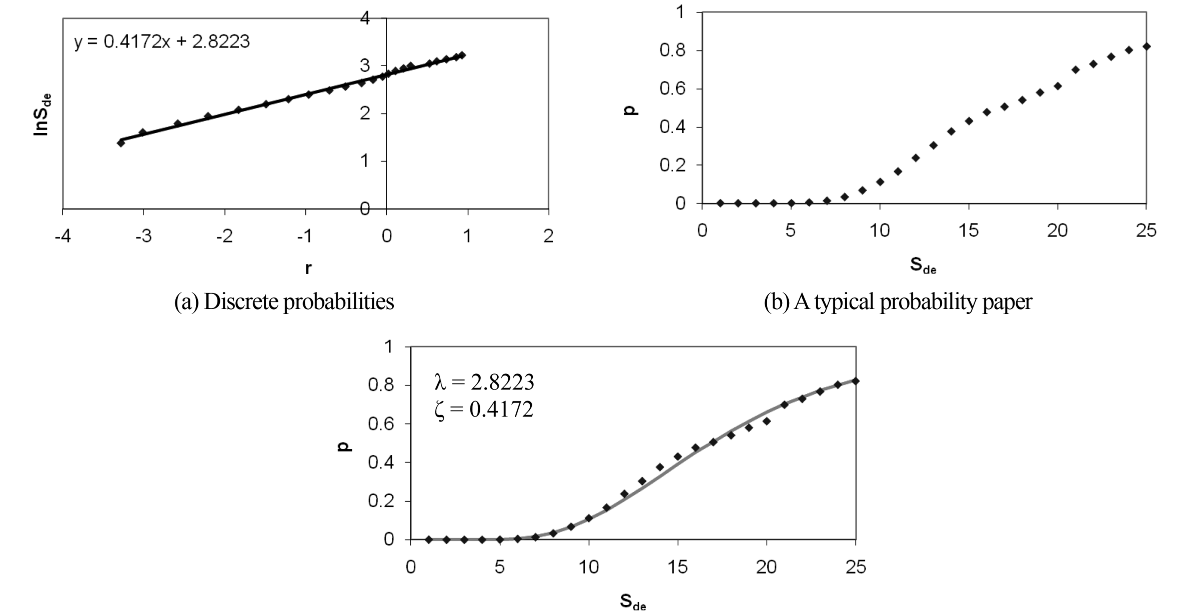

(a) Discrete probabilities (b) A typical probability paper

(c) Continuous form of fragility curve

Fig. 10 Constructing a typical fragility curve

The Eq. (11) is the equation of the approximate linear function of points of lognormal probability paper. The approximate straight line for determining the λ and ζ statistics was derived by using EXCEL. Mean continuous curve was derived by using the cumulative probabilities of spectral displacements (S_{de}) which were determined by using λ and ζ statistics.

12. Damage probabilities and fragility curves

The derived fragility curves are given in Fig. 11 and Fig. 12 for building A and B, respectively. In the figures, vertical axis "*p*" shows probability of exceeding target performance level.

Although the purpose of this study is not obtaining the fragility curves of the existing building stock in Turkey; the design earthquake given by TEC is selected so that damage probability level of

Table 6 Damage probabilities of the buildings

		BL	SSD30	SSD100	SSD30M2	SSD30M6	SSD100M2	SSD100M6
Building A	Immediate Occupancy	0.889	0.851	0.828	0.991	0.990	0.990	0.991
	Life Safety	0.322	0.327	0.278	0.807	0.826	0.800	0.828
	Collapse Prevention	0.010	0.028	0.018	0.266	0.317	0.286	0.347
Building B	Immediate Occupancy	0.992	0.975	0.980	0.996	0.994	0.996	0.940
	Life Safety	0.817	0.778	0.776	0.944	0.938	0.947	0.943
	Collapse Prevention	0.222	0.340	0.297	0.690	0.721	0.721	0.751

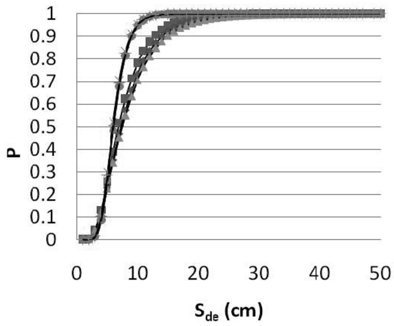

(a) Fragility curves for "Immediate Occupancy" performance level

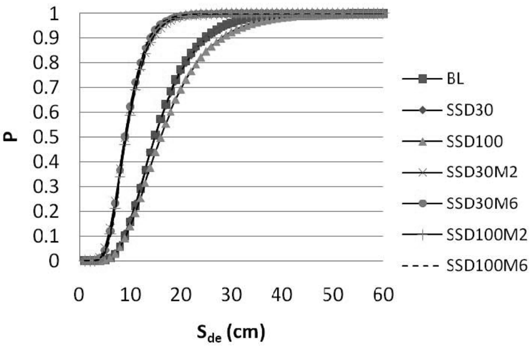

(b) Fragility curves for "Life Safety" performance level

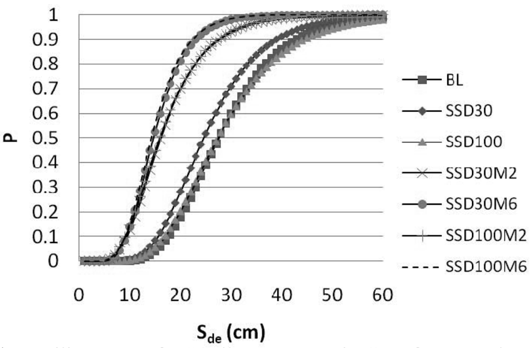

(c) Fragility curves for "Collapse Prevention" performance level

Fig. 11 Fragility curves of Building A

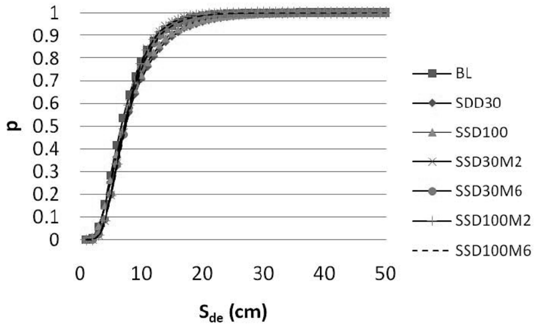

(a) Fragility curves for "Immediate Occupancy" performance level

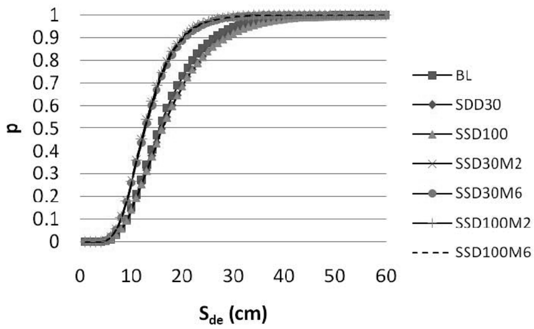

(b) Fragility curves for "Life Safety" performance level

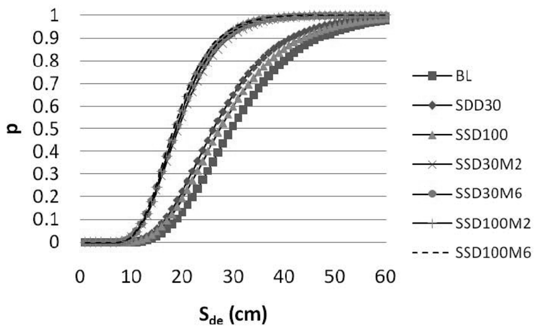

(c) Fragility curves for "Collapse Prevention" performance level

Fig. 12 Fragility curves of Building B

considered buildings can be compared. Table 6 shows the damage probability of each considered model under the effect of design earthquake given by TEC. These probabilities are also shown in the Fig. 13 for comparison of damage probability of each considered models for both sample buildings.

Building A has higher ductility and strength comparing to Building B. Thus, it is assumed that Building A is represented by the model SSD100M6 ($\gamma = 100$ and $u_c/u_y = 6$) while Building B is represented by the model SSD30M2 ($\gamma = 30$ and $u_c/u_y = 2$). It is worthy to note that the assumptions

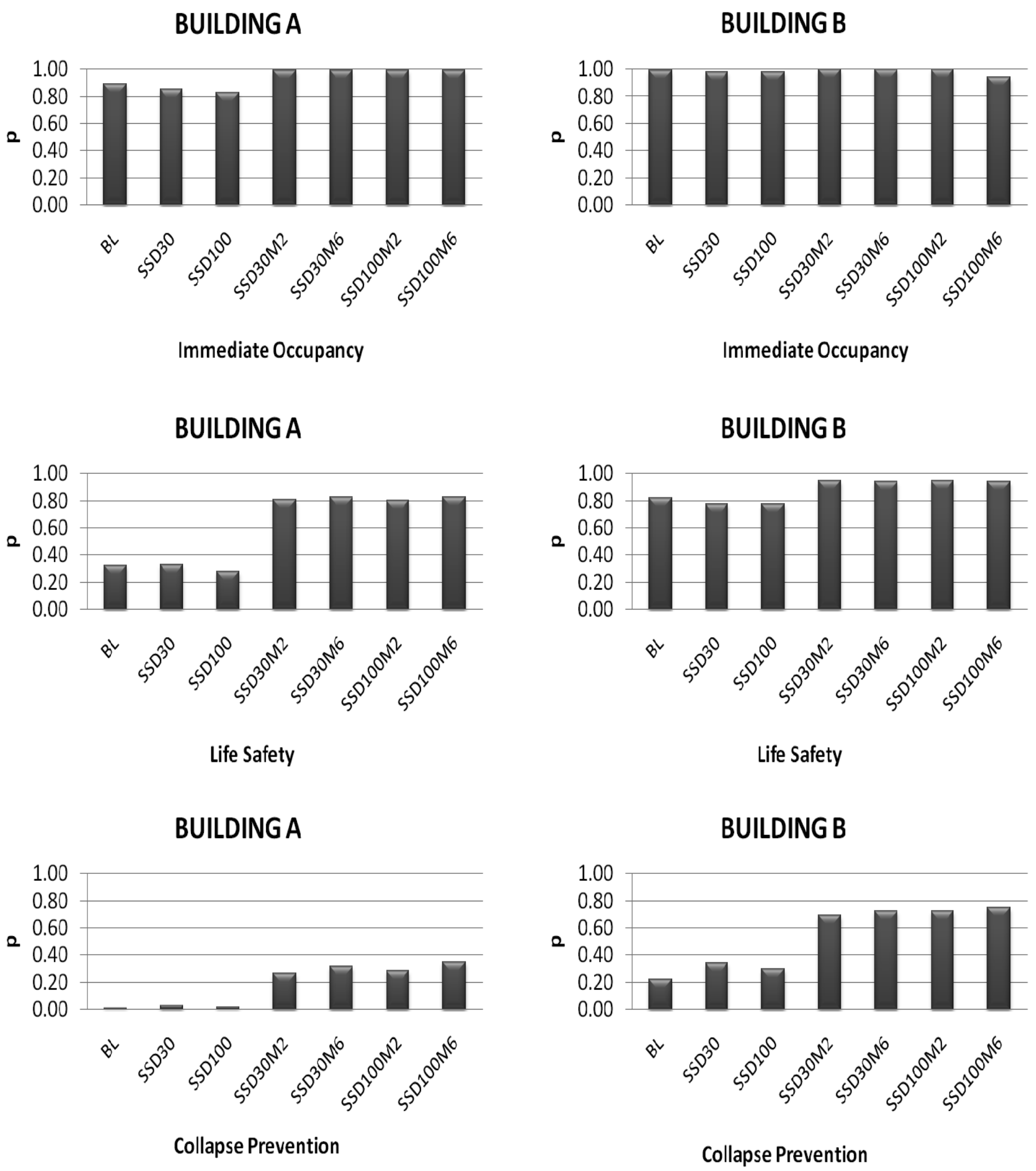

Fig. 13 Damage probabilities of each considered models for both sample buildings

mentioned above are subjective.

Fig. 14 shows the damage probability of considered buildings based on the aforementioned assumptions.

13. Conclusions

According to the results, damage probability is generally higher for the building which was

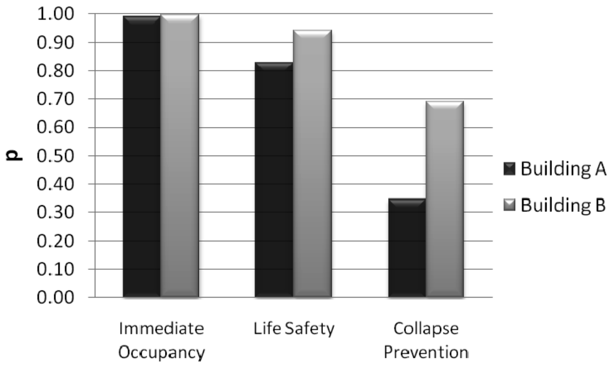

Fig. 14 Damage probabilities of the buildings for target performance levels

designed according to TEC-1975 (Building B) than that was designed according to TEC-2007 (Building A) as it is expected since the latter one has higher level of strength and ductility.

As it can be seen from the Fig. 14, probability of exceeding immediate occupancy performance level under the effect of design earthquake is almost same for both two buildings. However, the difference between damage probabilities of two considered buildings becomes more evident with increasing level of damage, since high strength and ductility becomes an important requirement at the higher level of damage.

According to the damage probability of the buildings, some comparisons can be made for bilinear or stiffness and strength deteriorated hysteretic models. It is important to note that, these comparisons are valid for the types of buildings which were considered in this study. There is no significant difference between bilinear hysteretic model or cyclic deteriorated hysteretic models which is not considered in-cycle strength degradation. When in-cycle strength degradation is considered, damage probability increases significantly for all performance levels. However, that increase becomes more explicit especially for sever damages (see Fig. 13).

The following conclusions also can be drawn from the results of this study;

- When only cyclic strength degradation is considered ($u_c/u_y = \infty$), damage probability increases with decreasing γ (while γ decreases cyclic deterioration becomes rapid) for sever damages (collapse prevention).
- When in-cycle strength degradation is considered in addition to cyclic strength degradation, damage probability increases with increasing u_c/u_y for severe damage level for constant γ.
- When both cyclic and in-cycle strength degradation are taken into account, the effect of in-cycle strength degradation on damage probability is more significant comparing to cyclic strength degradation.

In conclusion, load – displacement curves which consider stiffness and strength deterioration should be considered for the derivation of fragility curves of reinforced concrete structures especially for severe damage level. In-cycle strength degradation is more dominant according to cyclic strength degradation. Thus, especially for the sever damage level not only cyclic strength degradation but also in-cycle strength degradation must be considered for derivation of fragility curves.

References

Ayoub, A. and Chenouda, M. (2009), "Response spectra of degrading structural systems", *Eng. Struct.*, **31**(7), 1393-1402.

Bartlett, F.M. and MacGregor, J.G. (1996), "Statistical analysis of the compressive strength of concrete in structures", *ACI Mater. J.*, **93**(2), 158-168.

Chenouda, M. and Ayoub, A. (2009), "Probabilistic collapse analysis of degrading Multi Degree of Freedom structures under earthquake excitation", *Eng. Struct.*, **31**(12), 2909-2921.

Clough, R.W. and Johnston, S.B. (1966), "Effect of stiffness degradation on earthquake ductility requirements", *Proceedeings of the Second Japan National Conference on Earthquake Engineering.*

Erberik, M.A. and Elnashai, S.A. (2003), "Seismic vulnerability of flat-slab structures", *Technical Report DS-9 Project (Risk Assessment Modeling) Mid-America Earthquake Center,* University of Illinois at Urbana-Champaign.

FEMA 440 (2005), Improvement of Nonlinear Static Seismic Analysis Procedures.

FEMA 356 (2000), Prestandart and Commentary for the Seismic Rehabilitation of Buildings.

Ibarra, L.F., Medina, R.A. and Krawinkler, H. (2005), "Hysteretic models that incorporate strength and stiffness deterioration", *Earthq. Eng. Struct. D.,* **34**(12), 1489-1511.

Ibarra, L.F. (2002), SNAP Program User Guide.

Jeong, S. and Elnashai, S.A. (2007a), "Fragility relationships for torsionally-imbalanced buildings using three-dimensional damage characterization", *Eng. Struct.*, **29**(9), 2172-2182.

Jeong, S. and Elnashai, S.A. (2007b), "Probabilistic fragility analysis parameterized by fundamental response quantities", *Eng. Struct.,* **29**(6), 1238-1251.

Karim, K.R. and Yamazaki, F. (2003), "A simplified method of constructing fragility curves for highway bridges", *Earthq. Eng. Struct. D.*, **32**(10), 1603-1626.

Kirçil, M.S. and Polat, Z. (2006), "Fragility analysis of mid-rise R/C frame buildings", *Eng. Struct.*, **28**(9), 1335-1345.

Krawinkler, H., Parisi, F., Ibarra, L.F., Ayoub, A. and Medina, R. (2000), "Development of a testing protocol for wood frame structures", CUREE Publication No. W-02.

Kwon, O. and Elnashai, S.A. (2006), "The effect of material and ground motion on the seismic vulnerability curves of RC structures", *Eng. Struct.,* **28**(2), 289-303.

Mahin, S.A. and Bertero V.V. (1975), "An evaluation of some methods for predicting seismic behavior of reinforced concrete buildings", *University of California at Berkeley Earthquake Engineering Research Center*, Report No. 75-5.

Maniyar, M.M., Khare, R.K. and Dhabal, R.P. (2009), "Probabilistic seismic performance evaluation of non-seismic RC frame buildings", *Struct. Eng. Mech.,* **33**(6), 725-745.

NCEER (1996), "IDARC 2D Version 4.0: A computer program for the inelastic damage analysis of buildings", *National Center of Earthquake Engineering Research*, Buffalo.

Otani, S. (1981), "Hysteresis model of reinforced concrete for earthquake response analysis", *J. of Fac. of Eng. Univ. of Tokyo,* **36**(2), 407-441.

PEER Strong Motion Database, http://peer.berkeley.edu/smcat/.

Rahnama, M. (1993), "Effect of soft soil and hysteresis model on seismic demands", PhD Thesis, Stanford University.

Senel, S.M. and Kayhan, A.H. (2010), "Fragility based damage assessment in existing precast industrial buildings: A case study for Turkey", *Struct. Eng. Mech.,* **34**(1), 39-60.

Turkish Earthquake Code (2007), The Ministry of Public Works and Settlement, Turkey.

Turkish Earthquake Code (1975), The Ministry of Public Works and Settlement, Turkey.